

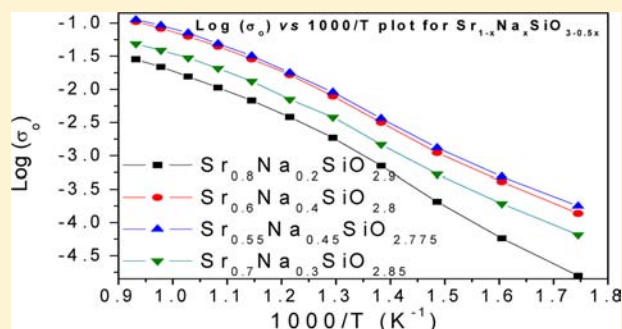
Monoclinic $\text{Sr}_{1-x}\text{Na}_x\text{SiO}_{3-0.5x}$: New Superior Oxide Ion Electrolytes

Preetam Singh and John B. Goodenough*

Texas Material Institute and Materials Science and Engineering Program, The University of Texas at Austin, Austin, Texas 78712, United States

S Supporting Information

ABSTRACT: Oxide ion electrolytes determine the temperature of operation of solid oxide fuel cells, oxygen separation membranes, and oxygen sensors. There is a strong incentive to lower their operating temperatures, in a solid oxide fuel cell, for example, from $T_{\text{op}} > 800\text{ }^\circ\text{C}$ to $T_{\text{op}} \approx 500\text{ }^\circ\text{C}$. The use of low-cost Na^+ rather than K^+ as the dopant in monoclinic SrSiO_3 (C12/C1) is shown to provide a larger solid solution range ($0 < x \leq 0.45$) in $\text{Sr}_{1-x}\text{Na}_x\text{SiO}_{3-0.5x}$ and to achieve an oxide ion conductivity $\sigma_o \geq 10^{-2}\text{ S}\cdot\text{cm}^{-1}$ by $525\text{ }^\circ\text{C}$ as a result of lowering the temperature of a smooth transition to full disorder of the mobile oxide ions. The $\text{Sr}_{1-x}\text{Na}_x\text{SiO}_{3-0.5x}$ electrolytes are much less hygroscopic than $\text{Sr}_{1-x}\text{K}_x\text{SiO}_{3-0.5x}$ and are stable with a nickel composite anode in $5\% \text{H}_2/\text{Ar}$ as well as with cathodes such as $\text{La}_{1-x}\text{Sr}_x\text{MnO}_{3-\delta}$ and $\text{Sr}_{0.7}\text{Y}_{0.3}\text{CoO}_{3-\delta}$ in air, which makes them candidate electrolytes for intermediate-temperature solid oxide fuel cells or for other applications of oxide ion electrolytes.



INTRODUCTION

Solid oxide ion electrolytes have several important applications.^{1–3} There is a strong incentive to lower their operating temperatures, in a solid oxide fuel cell (SOFC), for example, from $T_{\text{op}} > 800\text{ }^\circ\text{C}$ to $T_{\text{op}} \approx 500\text{ }^\circ\text{C}$. The most common oxide ion electrolytes have an oxygen-deficient fluorite or perovskite structure with oxygen transport by oxygen vacancies,^{4–9} but other structures supporting conduction of interstitial oxide ions are also known.^{10–21} The precise mechanistic model of oxide ion transport in rare-earth oxyapatites ($\text{RE}_{10}(\text{SiO}_4)_6\text{O}_3$),^{12–16} mainly $\text{La}_{9.33}\square_{0.67}(\text{SiO}_4)_6\text{O}_2$ and $\text{La}_8\text{Sr}_2(\text{SiO}_4)_6\text{O}_2$, has recently been studied at the atomic level by computer modeling techniques;¹⁶ it shows that the high ionic conductivity and low activation energy of $\text{La}_{9.33}\square_{0.67}(\text{SiO}_4)_6\text{O}_2$ are due to interstitial oxide ions with a zigzag pathway along the *c*-axis. The simulations demonstrate the importance of local relaxation of $[\text{SiO}_4]$ tetrahedra to assist in the facile conduction of interstitial oxide ions. Similarly the 2D-connected network of gallium oxide tetrahedra in the melilite structure $\text{La}_{1.54}\text{Sr}_{0.46}\text{Ga}_3\text{O}_{7.27}$ stabilizes oxide ion interstitials by local relaxation around them, affording an oxide ion conductivity of $0.02\text{--}0.1\text{ S cm}^{-1}$ over the $600\text{--}900\text{ }^\circ\text{C}$ temperature range.^{22,23}

Recently, we have reported fast oxide ion conduction in $\text{Sr}_{1-x}\text{K}_x\text{MO}_{3-0.5x}$ ($M = \text{Si, Ge}$) exhibiting a powder diffraction pattern that changes little with doping.²⁴ The structure of $\text{Sr}_3\text{Si}_3\text{O}_9$ consists of close-packed sheets of Sr^{2+} ions in trigonal-prismatic coordination separated by a layer containing Si_3O_9 complexes in which three SiO_4 units share corners in a planar array; two terminal oxygens per Si perpendicular to the plane coordinate the Sr^{2+} ions.^{24,25} Substitution of K^+ for Sr^{2+} introduces oxygen vacancies that, if located at a terminal position of a Si_3O_9 complex, would represent a steric hindrance

of corner sharing of an oxygen between Si_3O_9 complexes. Corner sharing would require a distortion of the Si_3O_9 complexes, and steric hindrance would represent a new principle for designing a solid oxide ion electrolyte. On the other hand, in light of the oxide ion conduction mechanism and structural features in Si/Ge apatites as well as the melilites, it was recognized that the driving force for forming corner sharing between complexes would be strong and corner-shared SiO_4 networks are flexible, so we could not rule out a reorganization into corner-shared Si_3O_9 complexes that would create mobile oxide ion interstitials. Corner sharing would eliminate the oxide ion vacancy, and the required rearrangements create another Si–O–Si bond between Si_3O_9 units with a resulting interstitial oxide ion as observed in the case of $\text{La}_{9.33}\square_{0.67}(\text{SiO}_4)_6\text{O}_2$.¹⁶ However, the X-ray diffraction (XRD) data indicated that such a reorganization would have to leave a layered structure commensurate with that of the parent structure. Moreover, these K-substituted oxides are hygroscopic at room temperature, which indicates that water is being absorbed into oxygen vacancies.

In this paper we report the use of smaller, less electropositive Na^+ rather than K^+ , which would reduce the steric hindrance; a larger solid solution range ($0 \leq x \leq 0.45$) in $\text{Sr}_{1-x}\text{Na}_x\text{SiO}_{3-0.5x}$ provides an oxide ion conductivity $\sigma_o \geq 10^{-2}\text{ S cm}^{-1}$ by $525\text{ }^\circ\text{C}$ as a result of lowering the temperature of a smooth transition to full disorder of the mobile oxide ions. These Na-substituted oxides are much less hygroscopic than K-substituted oxides. This result favors a high σ_o by creation of interstitial oxide ions rather than oxide ion vacancies, and a low water absorption at

Received: May 6, 2013

Published: June 20, 2013

room temperature is consistent with an oxygen interstitial conduction.

EXPERIMENTAL SECTION

$\text{Sr}_{1-x}\text{A}_x\text{SiO}_{3-0.5x}$ ($\text{A} = \text{Na}$ or K) and $\text{Sr}_{1-2x}\text{La}_x\text{Na}_x\text{SiO}_3$ ($x = 0.2$) samples were synthesized by solid-state reaction from a stoichiometric amount of mixed SrCO_3 , La_2O_3 , SiO_2 , K_2CO_3 , and Na_2CO_3 powders heated for 20 h ($\text{A} = \text{Na}$) at 1050 °C and at 1150 °C ($\text{A} = \text{K}$). The dry samples were obtained by slow furnace cooling to room temperature. For conductivity measurements, the resulting powders were made into pellets (typically ~0.2 cm in thickness and ~1 cm in diameter) by pressing the powder with 1 wt % poly(vinylbutyral) (PVB) at 5 GPa and firing for 20 h at 1050 °C for $\text{A} = \text{K}$ and at 1000 °C for $\text{A} = \text{Na}$.

The phase purity of the compounds appeared to be confirmed by powder XRD with a Philips X'pert diffractometer ($\text{Cu K}\alpha$ radiation, $\lambda = 1.5418$ Å) in Bragg–Brentano reflection geometry. A Rietveld structure refinement was carried out with the Fullprof program and the monoclinic SrSiO_3 (C12/C1) model; the required quantities of K/Na ions were placed randomly at Sr sites. The microstructures (shape and surfaces) of the powder and pellets were examined with scanning electron microscopy (SEM) at an accelerating voltage of 20 kV (JEOL, JSM-5610). The composition and apparent homogeneity of the compounds was confirmed by energy-dispersive X-ray (EDX) spectroscopy with a probe attached to the SEM instrument. Thermogravimetric analysis (TGA) of the samples was done in an air atmosphere (air flow 20 cm^3/min) with a heating rate of 2 °C/min.

Two-probe ac impedance measurements of oxide ion conductivity (σ_o) were made in air with a Solartron impedance analyzer (model 1287) operating in the frequency range from 1 Hz to 10 MHz with an ac amplitude of 10 mV. Two Pt blocking electrodes were made by coating Pt paste (from Heraeus) on the two faces of the pellets and baking at 800 °C for 1 h. All measurements were made on cooling from 800 to 300 °C. The conductivity was determined from the difference from the origin to the extrapolation of the intercept to the real Z' axis of a low-frequency semicircle or spike.

RESULTS AND DISCUSSION

The powder XRD patterns of Figure 1 show that the $\text{Sr}_{1-x}\text{A}_x\text{SiO}_{3-0.5x}$ ($\text{A} = \text{Na}$ or K) samples are single-phase to XRD in the interval $0.1 \leq x \leq 0.45$ for $\text{A} = \text{Na}$ and in the interval $0.1 \leq x \leq 0.35$ for $\text{A} = \text{K}$.²⁰ Without substitution of Na or K, SrSiO_3 does not form a single phase. Rietveld refinement of the XRD profile of $\text{Sr}_{0.55}\text{Na}_{0.45}\text{SiO}_{2.775}$ is shown in Figure 2. All the peaks in the recorded XRD profile match with reflections of the structure (see the green lines in Figure 2), and the fitted profiles also match well the observed XRD patterns. The structural parameters of different compositions of $\text{Sr}_{1-x}\text{A}_x\text{SiO}_{3-0.5x}$ ($\text{A} = \text{Na}$ or K) samples obtained from the Rietveld refinement of the powder XRD patterns are given in Table 1. The high R_{wp} parameter suggests the presence of oxygen vacancies (or interstitials) that disorder randomly the oxygen positions or the orientation of paired Si_6O_{17} groups, which cannot be exactly monitored with powder XRD. The compositions of the $\text{Sr}_{1-x}\text{A}_x\text{SiO}_{3-0.5x}$ ($\text{A} = \text{Na}/\text{K}$) samples were analyzed by EDX. SEM micrographs and the EDX profile of $\text{Sr}_{0.55}\text{Na}_{0.45}\text{SiO}_{2.775}$ (powder and pellet used for conductivity measurement) are given in Figure 3. The SEM study reveals that the powders are porous with grain sizes of 5–10 μm . However, the pellets were well-sintered, and the grains were in good contact with each other. The EDX study also confirms the composition and apparent homogeneity of the materials. The density of the pellets obtained by the Archimedes principle in water was ~97% of the theoretical density of the material.

Since SrSiO_3 could not be synthesized as a single monoclinic phase, we were not able to determine the oxide ion conductivity of the undoped sample. As previously reported,²⁰

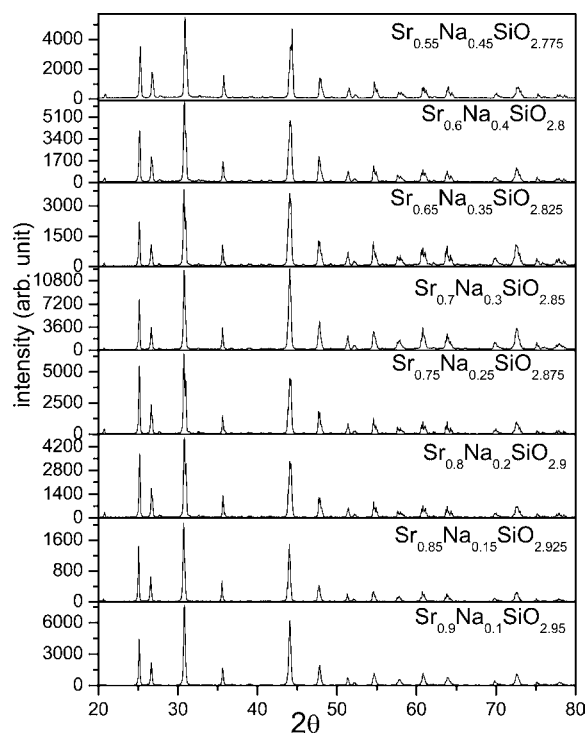


Figure 1. Powder XRD pattern for $\text{Sr}_{1-x}\text{Na}_x\text{SiO}_{3-0.5x}$ ($0.1 \leq x \leq 0.45$).

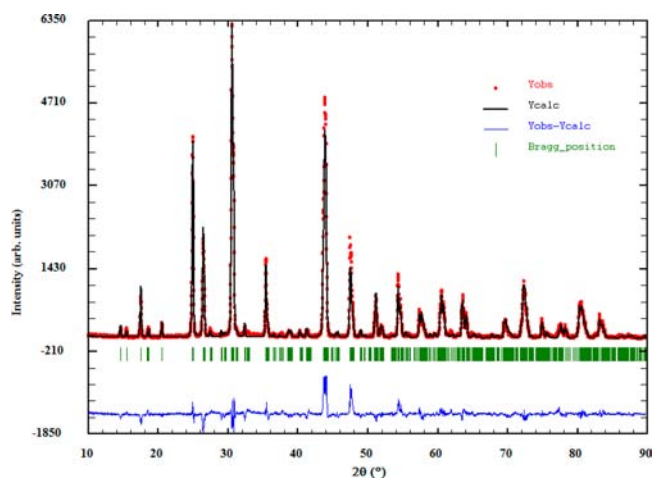
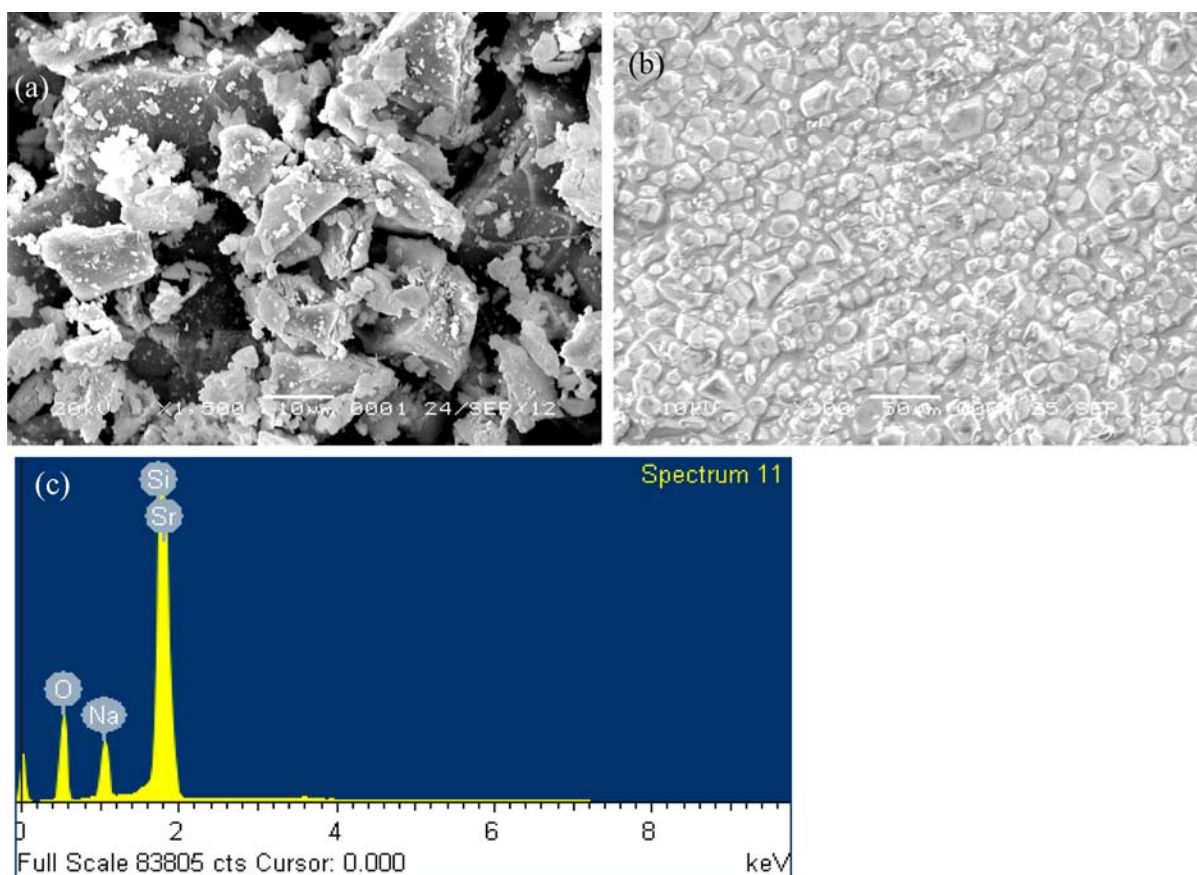


Figure 2. Observed XRD pattern and Rietveld refined profile of $\text{Sr}_{0.55}\text{Na}_{0.45}\text{SiO}_{2.775}$.

the $\text{Sr}_{1-x}\text{K}_x\text{SiO}_{3-0.5x}$ system exhibited a $\sigma_o = 7.5 \times 10^{-3} \text{ S cm}^{-1}$ at 800 °C (considerably smaller than the σ_o of $\text{Sr}_{1-x}\text{K}_x\text{Si}_{0.5}\text{Ge}_{0.5}\text{O}_{3-0.5x}$). We compare this result with that of $\text{Sr}_{1-x}\text{Na}_x\text{SiO}_{3-0.5x}$ shown in Figure 4, where $\sigma_o(T)$ increases with x over the range $0.1 \leq x \leq 0.45$; a $\sigma_o \approx 10^{-2} \text{ S cm}^{-1}$ is achieved at 525 °C for $x \geq 0.40$ ($\sigma_o = 1.79 \times 10^{-2} \text{ S cm}^{-1}$ at 550 °C for $x = 0.45$). The increase in O^{2-} conductivity with increasing x is a consistent trend (Figure 4), except for samples with $x = 0.3$, where the evolution of the cell volume with x (Table 1) is also anomalous. However, the results were repeatable, so it appears that there may be a change of arrangement of the $\text{SiO}_{4-\delta}$ linkages in the silicate layers at these compositions. The complex impedance spectrum for $\text{Sr}_{0.55}\text{Na}_{0.45}\text{SiO}_{2.775}$ at different temperatures is shown in Figure 5. The semicircle at high frequency reflects the response of the bulk and grain boundary; an apparent semicircle at low

Table 1. Structural Parameters of $\text{Sr}_{1-x}\text{A}_x\text{SiO}_{3-\delta}$ (A = Na or K)^a

compd	lattice parameters (Å)				cell vol (Å ³)	χ^2	R_f	R_{Bragg}	R_{wp}
	<i>a</i>	<i>b</i>	<i>c</i>	β					
SrSiO ₃ (ref 21)	12.333(2)	7.146(1)	10.885 (1)	111.57 (1)	892.12				
Sr _{0.9} K _{0.1} SiO _{2.95}	12.362 (1)	7.1435 (5)	10.9072 (3)	111.80 (1)	894.30	2.72	6.18	8.41	19.5
Sr _{0.85} K _{0.15} SiO _{2.925}	12.367 (1)	7.1439 (6)	10.9089 (8)	111.77 (1)	894.88	1.85	6.43	9.04	23.5
Sr _{0.8} K _{0.2} SiO _{2.9}	12.349 (1)	7.1528 (3)	10.9023 (3)	111.66 (1)	895.02	5.37	5.81	8.45	15.2
Sr _{0.75} K _{0.25} SiO _{2.875}	12.3464 (5)	7.1523 (3)	10.8934 (3)	111.61 (1)	894.55	4.17	8.36	10.8	20.1
Sr _{0.9} Na _{0.1} SiO _{2.95}	12.3533 (2)	7.1441 (5)	10.8975 (3)	111.51 (1)	893.25	3.57	8.97	14.2	29.6
Sr _{0.85} Na _{0.15} SiO _{2.925}	12.3576(6)	7.1421 (6)	10.9104(8)	111.32(1)	893.97	2.49	7.54	7.99	25.5
Sr _{0.8} Na _{0.2} SiO _{2.9}	12.3489(4)	7.1555 (2)	10.8973 (3)	111.57(1)	895.48	2.73	4.72	7.12	15.4
Sr _{0.75} Na _{0.25} SiO _{2.875}	12.3435(7)	7.1531(3)	10.8935(2)	111.57(1)	894.48	5.01	7.05	9.42	18.5
Sr _{0.7} Na _{0.3} SiO _{2.85}	12.3569(8)	7.1499(4)	10.9093(4)	111.72(1)	895.43	3.61	7.38	10.3	23.9
Sr _{0.65} Na _{0.35} SiO _{2.825}	12.3448(5)	7.1542(3)	10.8954(4)	111.58(1)	894.79	6.2	8.18	13.4	23.1
Sr _{0.6} Na _{0.4} SiO _{2.8}	12.3463(6)	7.1557(3)	10.8979(5)	111.58(1)	895.29	6.48	7.24	11.4	20.4
Sr _{0.55} Na _{0.45} SiO _{2.775}	12.3435(6)	7.1542(3)	10.8953(5)	111.58(1)	894.71	6.4	8.27	12.1	22.2

^aReference 25.Figure 3. SEM image of $\text{Sr}_{0.55}\text{Na}_{0.45}\text{SiO}_{2.775}$: (a) powder, (b) pellet. (c) EDX image of the pellet.

frequency is attributed to the electrode response. In the absence of separated high-frequency semicircles, we can only get the total conductivity and not the separate responses from the bulk and grain boundary. The absence of a semicircle at high frequencies (Figure 5) suggests that, owing to the high density of our pellet, the relative grain boundary contribution to the resistance is almost negligible at high temperatures. In the absence of any high-frequency semicircle in the plots, the intercept of the low-frequency semicircle or spike on the real (Z') axis represents the bulk crystal conductivity.²⁶ In the absence of a clear semicircle (Figure 5), we have also taken the

value of the intercept of the linear region of the curve to the real (Z') axis to determine the total ionic conductivity. The oxide ion conductivities (σ_o) and activation energies for $\text{Sr}_{1-x}\text{Na}_x\text{O}_{3-0.5x}$ at different temperatures are given in Table 2. The smooth change in activation energy centered at 550 °C in $\text{Sr}_{0.8}\text{K}_{0.2}\text{Si}_{0.5}\text{Ge}_{0.5}\text{O}_{2.9}$ ²⁰ is shifted to a little lower temperature in $\text{Sr}_{1-x}\text{Na}_x\text{SiO}_{3-0.5x}$ ($0.35 \leq x \leq 0.45$) to achieve a $\sigma_o > 10^{-2}$ S cm^{-1} at a lower temperature than in $\text{Sr}_{1-x}\text{K}_x\text{Si}_{1-y}\text{Ge}_y\text{O}_{3-0.5x}$.

We also performed TGA of our electrolytes to know the presence of absorbed water or hydroxide content in the sample, which may lead to a possible protonic conduction in the

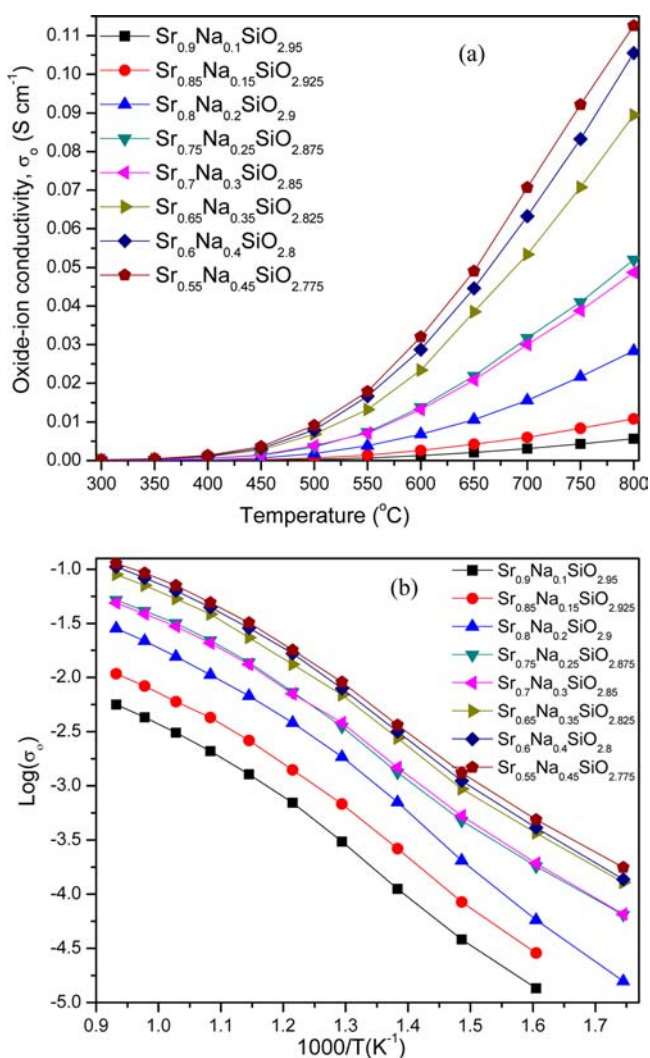


Figure 4. Oxide ion conductivity vs temperature (a) and $\log(\sigma_0)$ vs $1000/[T \text{ (K)}]$ (b) plots of $\text{Sr}_{1-x}\text{Na}_x\text{SiO}_{3-0.5x}$.

sample. The TGA plots of $\text{Sr}_{0.55}\text{Na}_{0.45}\text{SiO}_{2.775}$ (fresh and ~ 90 days in air) and of $\text{Sr}_{0.8}\text{K}_{0.2}\text{Si}_{0.5}\text{Ge}_{0.5}\text{O}_{2.9}$ are shown in Figure 6. In contrast to $\text{Sr}_{0.8}\text{K}_{0.2}\text{Si}_{0.5}\text{Ge}_{0.5}\text{O}_{2.9}$, which shows a total weight loss of $\sim 8\%$ up to 600°C , $\text{Sr}_{0.55}\text{Na}_{0.45}\text{SiO}_{2.775}$ shows little weight loss (fresh sample, $\sim 0.2\%$; old sample, $\sim 0.8\%$) up to 400°C ; above $400\text{--}800^\circ\text{C}$, no weight loss was observed. The absence of weight loss at high temperature ($>400^\circ\text{C}$) clearly suggests the absence of any protonic conductivity above 400°C in our sample owing to the absence of hydroxide ions from absorbed water. The continuous weight loss of $\sim 8\%$ up to 600°C and no weight loss above 600°C in $\text{Sr}_{0.8}\text{K}_{0.2}\text{Si}_{0.5}\text{Ge}_{0.5}\text{O}_{2.9}$ suggest the presence of oxide ion vacancies in the lattice that act as centers for water adsorption. However, the absence of or very little water adsorption even in a three month old $\text{Sr}_{0.55}\text{Na}_{0.45}\text{SiO}_{2.775}$ sample made it ambiguous whether oxygen vacancies were present in the lattice or oxygen interstitials were formed in the lattice. However, the anomalous conduction properties around $x = 0.3$ may indicate a transition from vacancy conduction to conduction by interstitial oxygen.

To confirm that the conductivity in our $\text{Sr}_{1-x}\text{Na}_x\text{SiO}_{3-0.5x}$ sample is mainly due to oxide ion and not Na ion or proton conductivity, we also measured the ionic conductivity of possible non-oxygen-deficient $\text{Sr}_{0.6}\text{La}_{0.2}\text{Na}_{0.2}\text{SiO}_3$; the samples show a very low ionic conductivity ($\sim 10^{-3} \text{ S cm}^{-1}$ at 800°C and $\sim 10^{-5} \text{ S cm}^{-1}$ at 600°C), whereas the $\text{Sr}_{0.8}\text{Na}_{0.2}\text{SiO}_{2.9}$ sample had a total ionic conductivity of $2.84 \times 10^{-2} \text{ S cm}^{-1}$ at 800°C and $3.83 \times 10^{-3} \text{ S cm}^{-1}$ at 500°C . However, as indicated earlier, pure oxygen-stoichiometric SrSiO_3 cannot be synthesized in a single monoclinic phase (it always formed along with other phases, for example, Sr_2SiO_4 and SiO_2).²⁷ $\text{Sr}_{0.6}\text{La}_{0.2}\text{Na}_{0.2}\text{SiO}_3$ was also not synthesized in a single monoclinic phase; instead, a small proportion of an oxide ion conducting La–Sr–Si–O apatite phase, mainly, $\text{La}_{4.32}\text{Sr}_{0.68}\text{Si}_3\text{O}_{13.16}$, was also formed (Figure S1, Supporting Information). We believe that some monoclinic oxygen-deficient $\text{Sr}_{1-x-y}\text{Na}_x\text{La}_y\text{SiO}_{3-0.5(x-y)}$ ($x > y$) region may also be present in the sample to compensate for the large La-

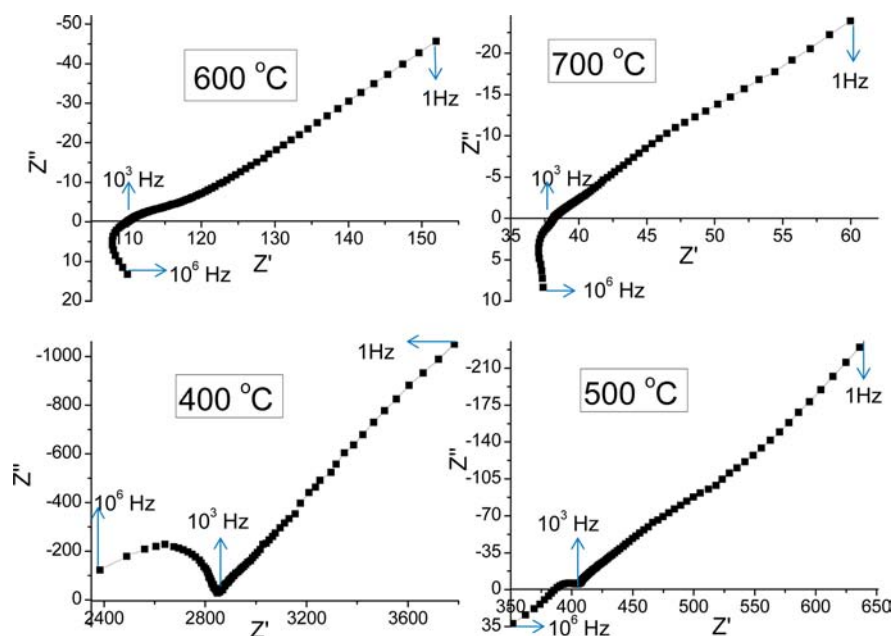


Figure 5. Complex impedance spectra for $\text{Sr}_{0.55}\text{Na}_{0.45}\text{SiO}_{3-\delta}$ at different temperatures.

Table 2. O²⁻ Conductivity (σ_0) of Sr_{1-x}A_xSiO_{3-0.5x} (A = Na or K) at Different Temperatures

compd	conductivity (S cm ⁻¹)						activation energy (E _a , eV)	
	550 °C	600 °C	650 °C	700 °C	750 °C	800 °C	high-temp region, ±0.05	low-temp region, ±0.07
Sr _{0.9} Na _{0.1} SiO _{2.95}	6.97 × 10 ⁻⁴	1.28 × 10 ⁻³	2.09 × 10 ⁻³	3.11 × 10 ⁻³	4.29 × 10 ⁻³	5.64 × 10 ⁻³	0.57	0.88
Sr _{0.85} Na _{0.15} SiO _{2.925}	1.4 × 10 ⁻³	2.62 × 10 ⁻³	4.28 × 10 ⁻³	5.98 × 10 ⁻³	8.37 × 10 ⁻³	1.08 × 10 ⁻²	0.53	0.87
Sr _{0.8} Na _{0.2} SiO _{2.9}	3.83 × 10 ⁻³	6.78 × 10 ⁻³	1.06 × 10 ⁻²	1.56 × 10 ⁻²	2.18 × 10 ⁻²	2.84 × 10 ⁻²	0.56	0.91
Sr _{0.75} Na _{0.25} SiO _{2.875}	7.36 × 10 ⁻³	1.38 × 10 ⁻²	2.19 × 10 ⁻²	3.17 × 10 ⁻²	4.1 × 10 ⁻²	5.2 × 10 ⁻²	0.44	0.76
Sr _{0.7} Na _{0.3} SiO _{2.85}	7.06 × 10 ⁻³	1.32 × 10 ⁻²	2.08 × 10 ⁻²	3.01 × 10 ⁻²	3.88 × 10 ⁻²	4.87 × 10 ⁻²	0.44	0.78
Sr _{0.65} Na _{0.35} SiO _{2.825}	1.33 × 10 ⁻²	2.34 × 10 ⁻²	3.85 × 10 ⁻²	5.34 × 10 ⁻²	7.07 × 10 ⁻²	8.95 × 10 ⁻²	0.48	0.76
Sr _{0.6} Na _{0.4} SiO _{2.8}	1.67 × 10 ⁻²	2.88 × 10 ⁻²	4.46 × 10 ⁻²	6.33 × 10 ⁻²	8.33 × 10 ⁻²	0.1055	0.49	0.77
Sr _{0.55} Na _{0.45} SiO _{2.775}	1.79 × 10 ⁻²	3.21 × 10 ⁻²	4.91 × 10 ⁻²	7.07 × 10 ⁻²	9.21 × 10 ⁻²	0.1126	0.48	0.78
Sr _{0.85} K _{0.15} SiO _{2.925}		3.69 × 10 ⁻⁴	8.26 × 10 ⁻⁴	1.58 × 10 ⁻³	3.01 × 10 ⁻³	4.65 × 10 ⁻³		
Sr _{0.8} K _{0.2} SiO _{2.9}		4.94 × 10 ⁻⁴	1.09 × 10 ⁻³	2.29 × 10 ⁻³	4.24 × 10 ⁻³	7.54 × 10 ⁻³	1.1	1.26

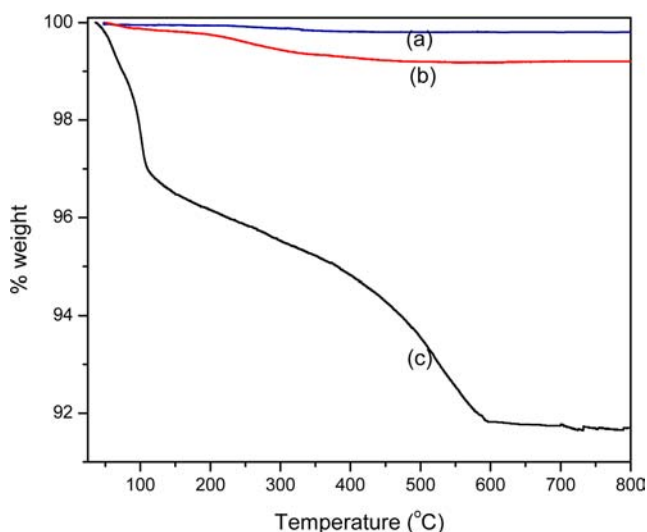


Figure 6. TGA plots for (a) fresh sample and (b) 90 day old sample of Sr_{0.55}Na_{0.45}SiO_{2.775} and (c) Sr_{0.8}K_{0.2}Si_{0.5}Ge_{0.5}O_{2.9} in air with a heating rate of 2 °C/min.

containing apatite phase to contribute to the oxide ion conductivity at higher temperature.

A nucleation of condensation of a mobile species is marked by an abrupt change in the activation energy at a specific temperature,⁹ e.g., 600 °C for La_{0.8}Sr_{0.2}Ga_{0.83}Mg_{0.17}O_{3-δ} (LSGM). In Sr_{1-x}A_xSiO_{3-0.5x}, the progressive trapping out of the mobile oxide ions with decreasing temperature occurs at a range of different trapping energies. The increase in σ_0 with x is suggestive of a percolation process for a more conductive phase associated with rearrangements of a corner-shared network of SiO₄ units. The larger solid solution range of Na allows for a larger volume fraction of the conductive phase. Whether the large alkali-metal ion hinders the formation of Si₃O₉ dimers on loss of oxygen or dimer formation creates interstitial oxygen remains an open question. As demonstrated in previous studies of conduction by interstitial oxide ions in Si/Ge apatites and in Ga-containing melilite, large cations exhibiting variable coordination numbers can provide the flexibility needed to accommodate mobile interstitial oxide ions created by cooperative network distortions; local relaxation of the MO₄ tetrahedra forms a larger space for interstitial oxide ions.¹²⁻¹⁶ A systematic investigation by means of differential thermal analysis and temperature-dependent powder X-ray diffraction has revealed that, in Rb₁₀Si₆O₁₇, the dimeric anion [Si₆O₁₇]¹⁰⁻ is formed by condensation of the [Si₃O₉]⁶⁻ anions of

Rb₆Si₃O₉.²⁸ Further study is needed to determine the character of the oxide ion conduction in Sr_{1-x}A_xSiO_{3-0.5x} (A = Na or K).

We also studied the thermal and chemical stability of the Sr_{1-x}A_xSiO_{3-0.5x} (A = Na or K) oxide ion electrolytes against various anode and cathode oxides to determine their applicability to an intermediate-temperature solid oxide fuel cell (IT-SOFC). Sr_{1-x}A_xSiO_{3-0.5x} (A = Na or K) is stable at 800 °C against a NiO electrolyte composite anode in a reducing atmosphere as well as cathodes such as La_{0.8}Sr_{0.2}MnO_{3-δ} and Sr_{0.7}Y_{0.3}CoO_{3-δ} in air. XRD patterns shown in Figures S2-S4 (Supporting Information) demonstrate that physical mixtures of the electrolyte (Sr_{0.55}Na_{0.45}SiO_{2.775}) and these cathodes and anode are stable even after heating at 800 °C for 12 h in air or a reducing atmosphere, respectively. The small variations in the powder X-ray pattern are due to the preferred orientation of the layered Sr_{0.55}Na_{0.45}SiO_{2.775} oxide.

In conclusion, compositions of the Sr_{1-x}Na_xSiO_{3-0.5x} system offer competitive oxide ion conductivities in the intermediate temperature range 500 °C < T < 800 °C, which makes them candidate electrolytes for an IT-SOFC or for other applications of oxide ion conductors. These electrolytes are stable at T = 800 °C with a nickel composite anode in a 5% H₂/argon atmosphere as well as with cathodes such as La_{1-x}Sr_xMnO_{3-δ} and Sr_{0.7}Y_{0.3}CoO_{3-δ} in air.

■ ASSOCIATED CONTENT

📄 Supporting Information

Powder XRD data for several samples. This material is available free of charge via the Internet at <http://pubs.acs.org>.

■ AUTHOR INFORMATION

✉ Corresponding Author

jgoodenough@mail.utexas.edu

Notes

The authors declare no competing financial interest.

■ ACKNOWLEDGMENTS

We thank the Robert A. Welch Grant Foundation (Grant No. F-1066) of Houston, TX, for financial support.

■ REFERENCES

- (1) Aguadero, A.; Fawcett, L.; Taub, S.; Woolley, R.; Wu, K.; Xu, N.; Kilner, J. A.; Skinner, S. J. *J. Mater. Sci.* **2012**, *47*, 3925.
- (2) Malavasi, L.; Fisher, C. A. J.; Islam, M. S. *Chem. Soc. Rev.* **2010**, *39*, 4370.
- (3) Jacobson, A. J. *Chem. Mater.* **2010**, *22*, 660.
- (4) Steele, B. C. H.; Heinzel, A. *Nature* **2001**, *414*, 345.

- (5) Goodenough, J. B. *Annu. Rev. Mater. Res.* **2003**, *33*, 91.
- (6) Boivin, J. C.; Mairesse, G. *Chem. Mater.* **1998**, *10*, 2870.
- (7) Hideaki, I.; Hiroaki, T. *Solid State Ionics* **1996**, *83*, 1.
- (8) Ishihara, T.; Matsuda, H.; Takita, Y. *J. Am. Chem. Soc.* **1994**, *116*, 3801.
- (9) Feng, M.; Goodenough, J. B. *Eur. J. Solid State Inorg. Chem.* **1994**, *31*, 663.
- (10) Nakayama, S.; Kageyama, T.; Aono, H.; Sadaoka, Y. *J. Mater. Chem.* **1995**, *5*, 1801.
- (11) Tao, S.; Irvine, J. T. S. *Mater. Res. Bull.* **2001**, *36*, 1245.
- (12) Abram, E. J.; Sinclair, D. C.; West, A. R. *J. Mater. Chem.* **2001**, *11*, 1978.
- (13) Arikawa, H.; Nishiguchi, H.; Ishihara, T.; Takita, Y. *Solid State Ionics* **2000**, *136*, 31–37.
- (14) Leon-Reina, L.; Losilla, E. R.; Martínez-Lara, M.; Bruque, S.; Aranda, M. A. G. *J. Mater. Chem.* **2004**, *14*, 1142.
- (15) Leon-Reina, L.; Losilla, E. R.; Martínez-Lara, M.; Carmen Martín-Sedeño, M.; Bruque, S.; Núñez, P.; Sheptyakov, D. V.; Aranda, M. A. G. *Chem. Mater.* **2005**, *17*, 596.
- (16) Tolchard, J. R.; Islam, M. S.; Slater, P. R. *J. Mater. Chem.* **2003**, *13*, 1956.
- (17) Esaka, T.; Minaai, T.; Iwahara, H. *Solid State Ionics* **1992**, *57*, 319–325.
- (18) Lacerda, M.; Irvine, J. T. S.; Glasser, F. P.; West, A. R. *Nature* **1988**, *332*, 525.
- (19) Fukuda, K.; Asaka, T.; Hamaguchi, R.; Suzuki, T.; Oka, H.; Berghout, A.; Be-chade, E.; Masson, O.; Julien, I.; Champion, E.; Thoma, P. *Chem. Mater.* **2011**, *23*, 5474–5483.
- (20) Wei, F.; Baikie, T.; An, T.; Schreyer, M.; Kloc, C.; White, T. J. *J. Am. Chem. Soc.* **2011**, *133*, 15200–15211.
- (21) Panchmatia, P. M.; Orera, A.; Rees, G. J.; Smith, M. E.; Hanna, J. V.; Slater, P. R.; Islam, M. S. *Angew. Chem., Int. Ed.* **2011**, *50*, 9328–9333.
- (22) Kuang, X.; Green, M. A.; Niu, H.; Zajdel, P.; Dickinson, C.; Claridge, J. B.; Jantsky, L.; Rosseinsky, M. J. *Nat. Mater.* **2008**, *7*, 498–504.
- (23) Tealdi, C.; Mustarelli, P.; Islam, M. S. *Adv. Funct. Mater.* **2010**, *20*, 3874–3880.
- (24) Singh, P.; Goodenough, J. B. *Energy Environ. Sci.* **2012**, *5*, 9626–9631.
- (25) Nishi, F. *Acta Crystallogr.* **1997**, *C53*, 534.
- (26) Jackowska, K.; West, A. R. *J. Mater. Sci.* **1983**, *18*, 2380–2384.
- (27) Ueno, A.; Hayashi, S.; Okada, K.; Otsuka, N. *J. Mater. Sci. Lett.* **1990**, *9*, 9–12.
- (28) Hoffmann, S.; Fassler, T. F. *Inorg. Chem.* **2006**, *45*, 7968–7972.